

The Relationship Between a Galaxy's Star Formation Rate and its Black Hole Accretion Rate

Victoria Song

Abstract

Active Galactic Nuclei (AGN), though only comprising a small percentage of the total galaxy mass, are believed to play an integral role in star formation, as suggested by theories developed in recent years. Furthermore, a galaxy's star formation likely contributes to its overall shape. After all, disk galaxies tend to be younger and more gas-rich than their elliptical counterparts, so they are likely to have higher star formation rates. We hypothesize that AGN hosts tend to be disk galaxies. By cross-matching morphology data with AGN data, this study aims to examine the relationship between AGN host galaxies, their star formation rates, black hole accretion rates, and their morphologies.

1. Introduction

Supermassive black holes (SMBHs), though only reaching up to ~0.5% of the host galaxy mass once fully evolved to present day, may play an important role in shaping the overall structure of their host galaxy. Galactic morphology remains at the forefront of modern astronomical research because it could provide insight on the history of the universe and map out the properties of our own galaxy, the Milky Way.

Active Galactic Nuclei (AGN) are SMBHs characterized by a uniquely high accretion rate. AGN are extraordinarily energetic and luminous, reaching up to 10^{15} solar luminosities, which makes them more luminous than their host galaxies. Although only a handful of galaxies in the modern cosmological era (past 1 billion years) host AGN, all galaxies are suspected to have undergone an AGN phase during their lifetimes.

Models and classification schemes of AGN are currently under development, but all AGN share the same basic anatomy. A SMBH resides at the center of the AGN. Surrounding particles lose angular momentum via friction, allowing them to fall into the center black hole through the formation of an accretion disk. A cool cloud of molecular gas and dust called the “dusty torus” then encompasses this region. Plasma spouts out the poles of the SMBH in the form of relativistic jets, which may help redistribute gas throughout the galaxy to fuel star formation. Regardless of the jets' impact on star formation, it is reasonable to assume that AGN, though relatively small and compact when compared to the rest of the galaxy, may be linked to the greater galactic structure due to their immense energy. The purpose of this paper is to explore the relationship between the presence of AGN and other processes that happen around the galaxy through the use of computational data analysis.

2. Methodology

Galaxies in the past were not only more active in forming stars and growing their black holes, but they were also heavily dust obscured. Therefore, star formation rates (SFR) and black hole accretion rates (BHAR) must be derived from a galaxy's infrared data to more accurately describe these processes in dusty galaxies. Although SFR values are usually derived from UV or optical data, infrared data serves as a better indicator for star formation in this case because radiation emitted at shorter wavelengths, especially in dusty galaxies, are absorbed by nearby dust particles. On the other hand, the radiation is re-emitted by the dust as infrared waves, which telescopes can accurately detect. Star formation occurs in cold, molecular regions of gas, which are kept cold by surrounding dust. Because dust is a good indicator of star formation, tracking the dust via infrared data is also optimal for obtaining SFR.

To calculate SFR, data from the CANDELS survey was used. The CANDELS survey was comprised of data for galaxies in COSMOS (COS), GOODS (GDS), Extended Groth Strip (EGS), and Ultra Deep Survey (UDS). Initially, the CANDELS data table included only total infrared luminosity ($8 \mu\text{m}$ – $1000 \mu\text{m}$) and fraction of the luminosity emitted by the AGN in the mid infrared spectrum ($5 \mu\text{m}$ – $15 \mu\text{m}$). These two quantities were used to deduce the SFR through other values, namely, total AGN fraction in the infrared, total luminosity emitted by the AGN in the infrared, total luminosity emitted by star formation in the infrared, and finally, SFR. Before performing these calculations, the CANDELS data table needed to be modified so that galaxies that fall below the limiting magnitude were removed. The limiting magnitude refers to the faintest objects that can be detected with the telescope. If the CANDELS data table had such an object, it would arbitrarily assign the object an s24 micron flux density, which acts as a filler and is not the actual flux density. Thus, the following s24 micron flux densities were removed from the data table:

$$\text{GDS: s24} = 0.020 \text{ mJy}$$

$$\text{UDS: s24} = 0.030 \text{ mJy}$$

$$\text{COS: s24} = 0.023 \text{ mJy}$$

$$\text{EGS: s24} = 0.050 \text{ mJy}$$

Once this change has been completed, the total AGN fraction was then computed from mid-infrared AGN fraction via this formula from Kirkpatrick et al. (2015):

$$f_{agn} = (0.66 \pm 0.09) \times f_{agn(mir)} - (0.035 \pm 0.07) \times f_{agn(mir)} \quad (1)$$

where f_{agn} represents the total AGN fraction and $f_{agn(mir)}$ represents the AGN fraction in the mid-infrared [1]. f_{agn} was used to calculate the total infrared luminosity emitted by the AGN:

$$L_{agn} = f_{agn} \times L_{IR} \quad (2)$$

Where L_{agn} represents the total infrared luminosity emitted by the AGN and L_{IR} is the total infrared luminosity of the galaxy as provided by the CANDELS data table. The infrared luminosity emitted by star formation is simply the difference between the total infrared luminosity of the galaxy and that of the AGN, as follows:

$$L_{sf} = L_{IR} - L_{agn} \quad (3)$$

Where L_{sf} represents the total infrared luminosity from star formation. Finally, SFR is calculated from L_{sf} using a relationship empirically derived by Kennicutt (1998): [2]

$$SFR [M_\odot \text{ yr}^{-1}] = 4.5 \times 10^{-44} L_{sf} \quad (4)$$

A similar procedure was used to calculate BHAR. Total luminosity emitted in the x-ray and bolometric luminosity were needed to get the answer. With L_{agn} obtained in Equation 2, x-ray luminosity could be obtained via the following conversion from Kirkpatrick et al. (2017):

$$\log \frac{L_x}{L_{agn}} = 28.629 - 0.661 \times \log L_{agn} \quad (5)$$

Where L_x is the x-ray luminosity [3]. L_x can then be used to calculate L_{bol} , the bolometric luminosity, in the following relationship from Hopkins et al. (2007): [4]

$$L_{bol} = -9.25 + 1.25L_x \quad (6)$$

Ultimately, BHAR could be calculated from L_{bol} using the equation below from Sun et al. (2015):

$$\dot{M} = \frac{(1 - \eta)L_{bol}}{\eta c^2} \quad (7)$$

Where \dot{M} represents the accretion rate, c represents the speed of light in vacuum, and η represents the efficiency at which material is accreted. In this case, η is assumed to be 10%, well below the Eddington limit. Equation 7 is another form of Einstein's $E = mc^2$, as it too describes the conversion of energy into mass.

In addition to calculating the BHAR from infrared data, BHAR values were also calculated directly from x-ray data. X-ray data files from the four fields of CANDELS were matched with the infrared CANDELS data table, ultimately producing a sample of approximately 200 galaxies. Although the procedure for both infrared and x-ray calculations was the same, BHAR values derived from x-ray data were higher than their infrared counterparts. Figure 1 shows the correlation between these two variables.

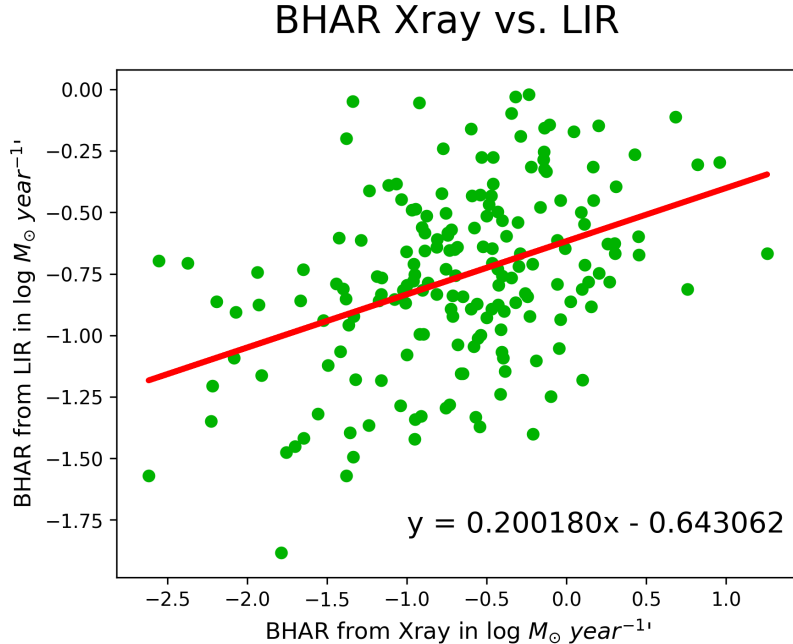


Figure 1. The plot shows BHAR values derived from x-ray (x-axis) as they compare with BHAR values derived from infrared (y-axis). The data are the green points, and the line of best fit is the red line. All x-ray derived BHAR values are higher than their infrared counterparts. A linear relationship was fitted to the data; BHAR from infrared increases with BHAR from x-ray in the form $y=0.200180x - 0.643062$, as displayed on the graph.

3. Results and Discussion

In the end, SFR and BHAR data was obtained for approximately 2000 galaxies in CANDELS. The data were then conjoined with FITS files containing more information on the respective CANDELS galaxies. Several plots were made to compare the properties of each galaxy within this sample.

Testing the correlation between a galaxy's stellar mass, SFR, and BHAR was a particular point of interest in this study. Graphs of Mstar (a galaxy's stellar mass) vs. SFR are shown in Figure 2. The graphs are sorted into three redshift bins. Cosmological redshift refers to an object's recession velocity or distance from our point of view. It could also describe specific cosmological epochs. For example, a redshift of $z=0.1$ would be considered the “local” universe and a redshift of $z=5$ would be considered the “early” universe. The CANDELS data were sorted into redshift bins to account for differences between different cosmological eras.

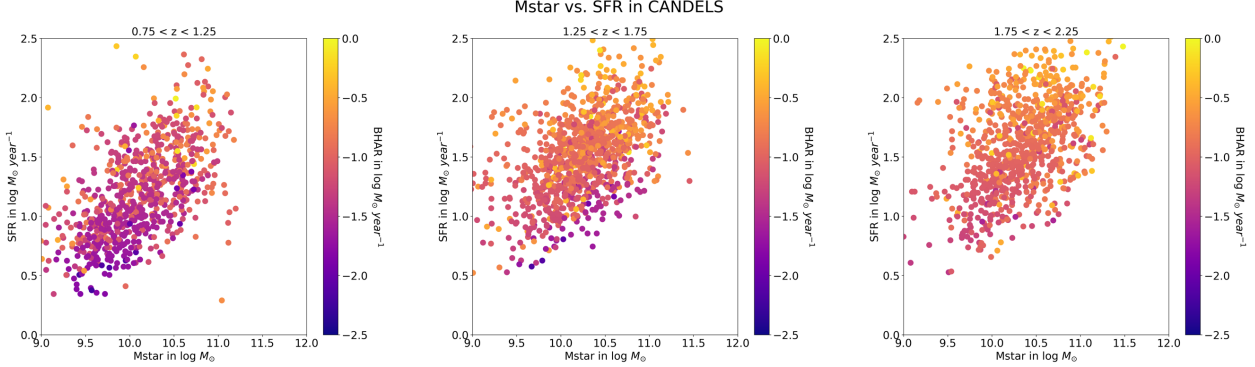


Figure 2. Plots of M_{star} (stellar mass) vs. SFR for all CANDELS galaxies. The galaxies are sorted into three redshift bins: 0.75 to 1.25 , 1.25 to 1.75 , and 1.75 to 2.25 . On all the plots, the stellar mass of the galaxy is graphed on the x -axis in units log solar masses, and the SFR is graphed on the y -axis in units log solar masses per year. The data is shaded by BHAR in units log solar masses per year. The plots seem to show that as stellar mass increases, so does SFR and BHAR . BHAR is also higher at higher redshifts, given the progressively yellower color.

Figure 3 shows another projection of the three variables.

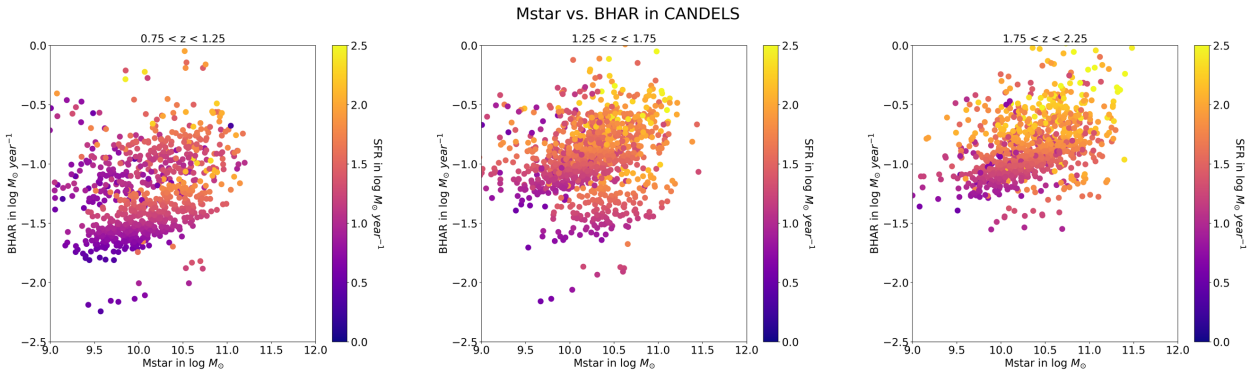


Figure 3. Plots of M_{star} (stellar mass) vs. BHAR for all CANDELS galaxies. As with Figure 2, the galaxies are sorted into three redshift bins. On all the plots, the stellar mass of the galaxy is graphed on the x -axis in units log solar masses, and the BHAR is graphed on the y -axis in units log solar masses per year. The data is shaded by SFR in units log solar masses per year. Once again, the plots seem to show that as stellar mass increases, so does SFR and BHAR . SFR is also higher at higher redshifts, given the progressively yellower color.

The graphs seem to exhibit some correlation among these three variables, albeit with a large amount of scatter. The separate clumps seen in Figures 2 and 3 could be attributed to differences between the fields surveyed. To eliminate this effect, each field (COS, EGS, GDS, and UDS) were parsed into different plots. (See the appendix for these graphs.)

Plots of M_{star} vs. BHAR were also made with x-ray data included, shown in Figure 4. All x-ray data points are higher than the great majority of BHAR values derived from infrared data. This disparity could have resulted from instrumental limitations (its sensitivity to pick up infrared waves vs. x-ray waves) or the conversion of infrared data to x-ray for the calculation of BHAR .

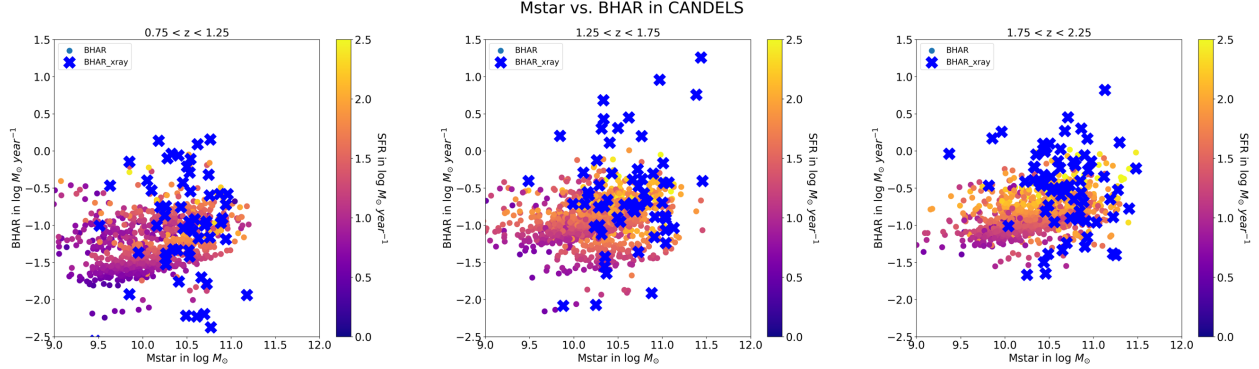


Figure 4. Plots of M_{star} (stellar mass) vs. BHAR with the x-ray data included. The stellar mass in log solar masses is graphed on the x-axis, and the BHAR in log solar masses per year is graphed on the y-axis. The data is shaded by SFR. The BHAR derived from x-ray is shown as blue x's on the graph.

SFR plots with the stellar main sequence were created to further examine the correlation between potential AGN host galaxies and their star formation rates. Figures 5 and 6 show the results of this investigation.

Figure 5 shows plots of stellar mass vs. SFR and is essentially Figure 2 with the main sequence included. Figure 5 does show that lower BHAR (shown as darker, purple points) tend to fall below both main sequence curves, which strengthens the initial claim that if a galaxy has a lower SFR, it would likely have a lower BHAR, and vice versa for higher values of each variable.

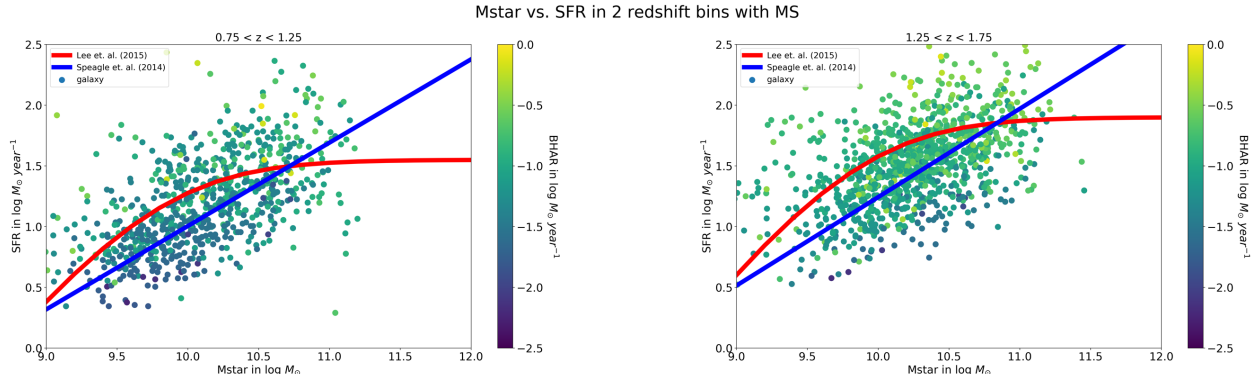


Figure 5. Plots of M_{star} vs. SFR, shaded by BHAR. M_{star} is in log solar masses, SFR is in log solar masses per year, and BHAR is in log solar masses per year. Main sequence star formation rate curves were also included. The red curve represents the main sequence projected by Lee et al. (2015), and the blue line represents the main sequence projected by Speagle et al. (2014).

Figure 6 shows a similar trend. Galaxies with higher specific SFR also tend to have higher BHAR/Mstar values, as shown by the cyan color near the upper-left hand region of the graph. As stellar mass increases, both specific SFR and BHAR/SFR decrease. The brighter cyan data points, which signify higher BHAR/Mstar, tend to lay above the main sequence in both redshift bins.

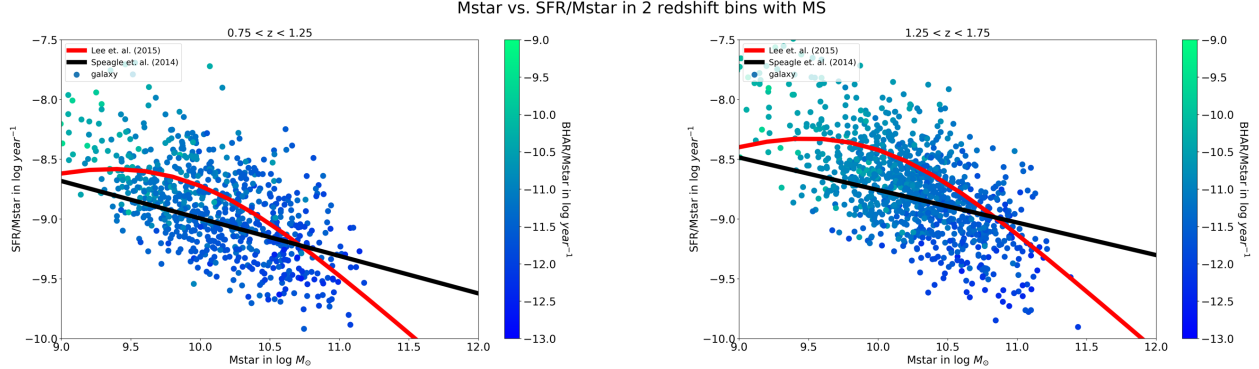


Figure 6. Plots of M_{star} vs. Specific SFR, shaded by BHAR/ M_{star} . M_{star} is in log solar masses, specific SFR is in log 1/ year, and BHAR/ M_{star} is in log 1/ year. Main sequence star formation rate curves were also included. The red and black curves are projections by Lee et al. (2015) and Speagle et al. (2014) respectively, but the formulas were rearranged to show the Main sequence for specific SFR rather than SFR.

In both Figures 5 and 6, two different projections of the main sequence are graphed to address a controversy. The projection by Speagle et al. (2014) is a simple linear correlation between a galaxy's stellar mass and star formation. The formula is shown below:

$$\log SFR = (0.84 \pm 0.02 - 0.026 \pm 0.003 \times t) \log M_* - (6.51 \pm 0.24 - 0.11 \pm 0.03 \times t) \quad (8)$$

where SFR represents the star formation rate, t represents the age of the universe in Gyr, and M_* represents a galaxy's stellar mass [5]. Using a linear equation, such as Equation 8, to extrapolate the main sequence for redshifts higher than $z=1$ is incorrect. However, speculation about a main sequence turnover at $z=1.5$ has not yet been confirmed. In addition, the relationship between stellar mass and SFR should plateau as stellar mass increases. After all, a higher stellar mass means that more of the gas supply within the galaxy has been consumed to fuel star formation. Equation 8, therefore, should be treated as an approximation of the main sequence so qualitative interpretations of the data may be performed.

The relationship from Lee et al. (2015) predicts that all galaxies follow a power-law at lower stellar masses, with a power-law slope ranging from 0.9 to 1.3. A turnover in the main sequence occurs at $\sim 10^{10}$ solar masses. The main sequence formula by Lee et al. (2015) is dependent on redshift and follows the basic structure seen below: [6]

$$S = S_0 - \log \left[1 + \left(\frac{10^{M_0}}{10^M} \right)^\gamma \right] \quad (9)$$

where S is the star formation rate in log solar masses per year (equivalent to $\log SFR$) along the main sequence, S_0 is maximum value of S in solar masses per year, M_0 is the turnover mass in solar masses, γ is the power-law slope, and M is the stellar mass in solar masses [6]. The values for S_0 , M_0 , and γ come from the extrapolation derived by Lee et al. (2015), seen in Figure 7:

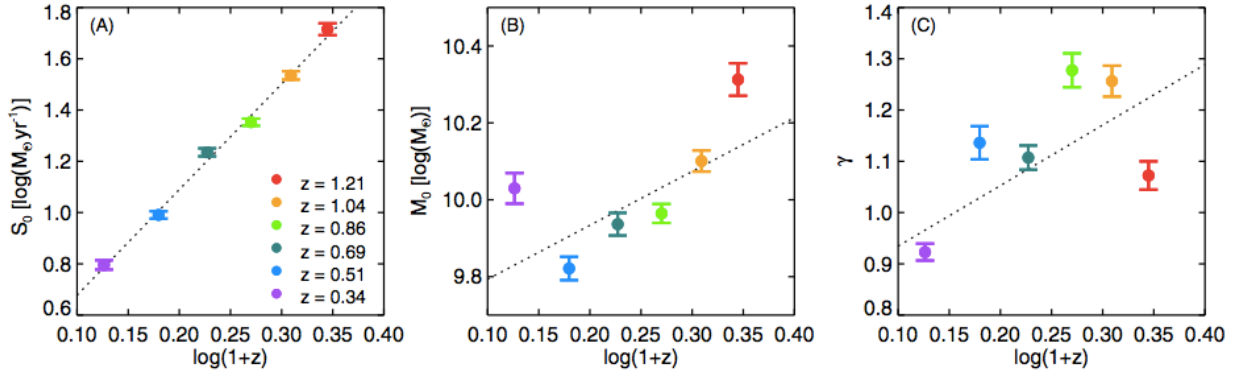


Figure 7. A figure from Lee et al. (2015) showing the extrapolations for different variables in Equation 9. The redshift in $\log(1+z)$ is graphed on the x-axis, and the variable (from left to right: S_0 , M_0 , and γ) on the y-axis. The data points collected by Lee et al. (2015) are color-coded to show their respective redshifts. [7]

The main sequence equations graphed in Figure 5 were obtained using the extrapolations presented in Figure 5. For galaxies with redshifts between $z=0.75$ and $z=1.25$, the average redshift $z=1$ was used to find S_0 , M_0 , and γ and produced the following equation: [8]

$$S = 1.55 - \log \left[1 + \left(\frac{10^{10.1}}{10^M} \right)^{1.25} \right] \quad (10)$$

For galaxies with redshifts between $z=1.25$ and $z=1.75$, the average redshift $z=1.5$ was used to find S_0 , M_0 , and γ and produced the following equation: [9]

$$S = 1.90 - \log \left[1 + \left(\frac{10^{10.2}}{10^M} \right)^{1.28} \right] \quad (11)$$

Overall, the positive correlation between SFR and BHAR was expected they are fueled by the same phenomena: the presence of a sufficient gas reservoir within the galaxy. The amount of gas in a galaxy begs the question of galactic structure. Whereas elliptical galaxies are gas-poor and old, spiral galaxies, on the other hand, are gas-rich and young. It is likely that AGN host galaxies are spiral galaxies since that would explain their black hole fueling mechanism. To determine if this was indeed the case, galaxies in the overlap between the GOODS-S field and CANDELS survey were plotted to see if their morphologies were linked with their BHAR. Figure 8 shows the results of this test.

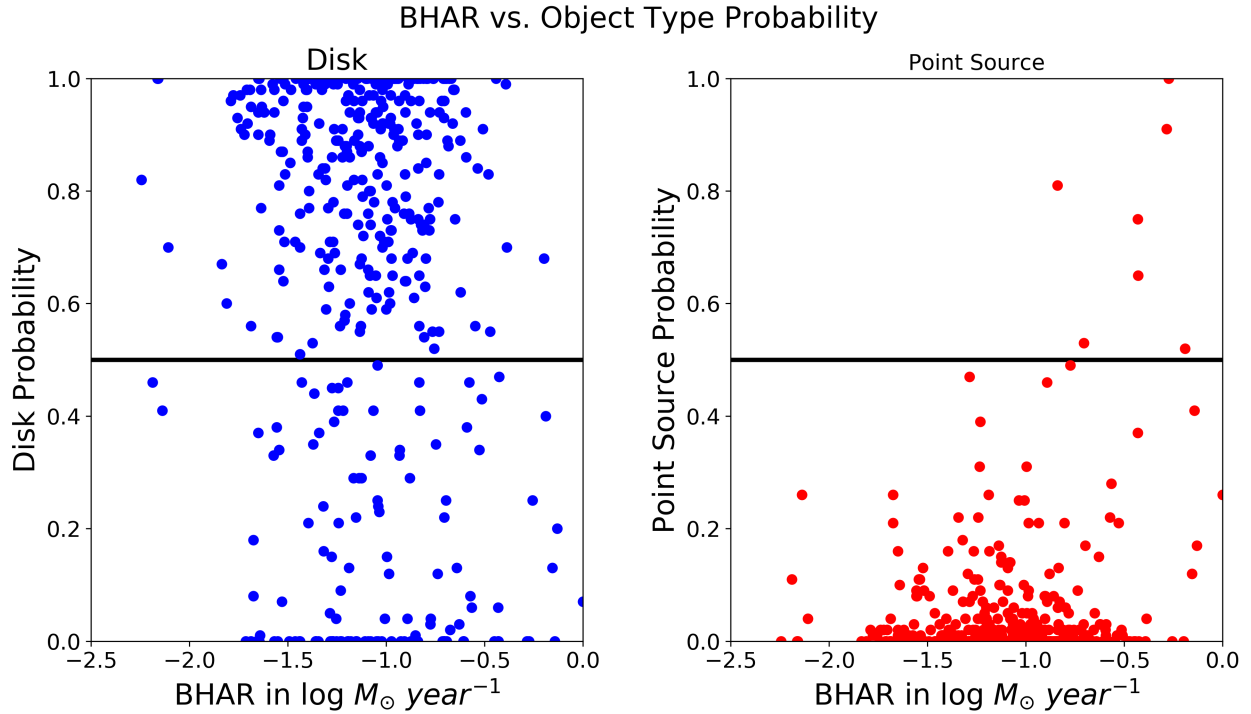


Figure 8. Graphs of BHAR vs. Object Type Probability, which is how likely the galaxies' morphologies are to be a certain shape. BHAR is graphed on the x-axis in units log solar masses per year. The left-hand graph has the probability that the object in question is a disk on the y-axis, on a scale of 0 to 1.0 refers to a probability of 0%, and 1 refers to a probability of 100%. The right-hand graph has the probability that the object is a point source on the y-axis using the same scale. The horizontal black line represents a 50% probability and is drawn for data interpretation.

The data points in Figure 8 come from approximately 400 galaxies, with morphology data taken directly from the Rainbow Navigator database. The probabilities were calculated via machine-learning. Surprisingly, the graphs seen in Figure 6 do not match the original hypothesis. No tangible correlation exists between BHAR and the probability that the object in question is a disk galaxy. The graph does show that most galaxies in the sample exhibit disk-like features, as shown by the number of data points above the 50% probability line compared to that of below. Likewise, the same objects have a low probability of being a point source. On the other hand, black hole accretion rate and point source probability seem to show some correlation, as point source probability rises with black hole accretion rate, though this correlation is very loose given the scatter. This result contradicts the classical picture of galaxy evolution and as such should be taken with a caveat. It is likely that the galaxies exhibiting a high probability of being point sources are actually disk galaxies because the brightness of the AGN may obscure the galaxy's morphology and prevent accurate classification. On the other hand, a different idea has emerged in recent years supporting the hypothesis that the majority of obscured black hole growth occurs alongside star formation. It is still possible that a galaxy's morphology is connected with its BHAR, but other means of experimentation must be used to confirm the relationship.

4. Conclusion

In summary, a positive correlation seems to exist between a galaxy's SFR and its BHAR. This is supported empirically by the data produced and theoretically by the fact that both SFR and BHAR are fueled by the presence of a sufficient gas reservoir within a galaxy. Future work remains to be done on the question of whether galactic morphology is also linked with these two variables. The morphology graphs shown in Figure 8 seem to disprove any connection between a galaxy's shape and its BHAR, but the data likely appears this way due to instrumental limitations of the telescope from which it was collected, as the extraordinary brightness of an AGN could easily obscure the true shape of its host galaxy. The possibility of a correlation between morphology and BHAR is yet to be verified through the use of other methods.

5. Acknowledgements

I would like to acknowledge Prof. Urry and Dr. Kirkpatrick for supervising, instructing, and helping me with my summer project on AGN, as well as the Yale Department of Astronomy and the Choate Science Research Program for their support.

References

1. Allison Kirkpatrick et al., The Role of Star Formation and an AGN in Dust Heating of z = 0.3-2.8 Galaxies. I. Evolution with Redshift and Luminosity, research report no. 814:9, 14, November 10, 2015, accessed November 15, 2017,
<http://iopscience.iop.org/article/10.1088/0004-637X/814/1/9/meta;jsessionid=64983E953F2B18C5F729C919A383648F.c2.iopscience.cld>.
2. Robert C. Kennicutt, Jr., Star Formation in Galaxies Along the Hubble Sequence, research report no. 9807187v1, 11, July 17, 1998, accessed November 15, 2017,
<http://arxiv.org/abs/astro-ph/9807187>.
3. Allison Kirkpatrick et al., "How Prevalent are Galaxies with Simultaneous Star Formation and Black Hole Growth at Cosmic Noon? Predictions for the James Webb Space Telescope" (unpublished manuscript, Yale University, New Haven, CT, June 15, 2017), 9.
4. Philip F. Hopkins, Gordon T. Richards, and Lars Hernquist, An Observational Determination of the Bolometric Quasar Luminosity Function, research report no. 654:731-753, 734, September 15, 2006, accessed October 30, 2017,
<http://iopscience.iop.org/article/10.1086/509629/fulltext/>.
5. J. S. Speagle et al., A Highly Consistent Framework for the Evolution of the Star-forming “Main Sequence” from z~ 0-6, research report no. 214:15, 1, September 18, 2014, accessed November 15, 2017, <http://iopscience.iop.org/article/10.1088/0067-0049/214/2/15/meta>.
6. Nicholas Lee et al., A Turnover in the Galaxy Main Sequence of Star Formation at M * ~ 10^10 Msun for Redshifts z < 1.3, research report no. 801:80, 6, March 5, 2015, accessed November 15, 2017, <http://iopscience.iop.org/article/10.1088/0004-637X/801/2/80/meta>.
7. Lee et al., A Turnover, 8.
8. Ibid.
9. Ibid.

Bibliography

Hopkins, Philip F., Gordon T. Richards, and Lars Hernquist. *An Observational Determination of the Bolometric Quasar Luminosity Function*. Research report no. 654:731-753.

September 15, 2006. Accessed October 30, 2017.

<http://iopscience.iop.org/article/10.1086/509629/fulltext/>.

Kennicutt, Robert C., Jr. *Star Formation in Galaxies Along the Hubble Sequence*. Research report no. 9807187v1. July 17, 1998. Accessed November 15, 2017.

<http://arxiv.org/abs/astro-ph/9807187>.

Kirkpatrick, Allison, Stacey Alberts, Alexandra Pope, Guillermo Barro, Matteo Bonato, Dale D. Kocevski, Pablo Pérez-González, George Rike, Lucia Rodríguez-Munoz, and Anna Sajina. "How Prevalent are Galaxies with Simultaneous Star Formation and Black Hole Growth at Cosmic Noon? Predictions for the James Webb Space Telescope." Unpublished manuscript, Yale University, New Haven, CT, June 15, 2017.

Kirkpatrick, Allison, Alexandra Pope, Anna Sajina, Eric Roebuck, Lin Yan, Lee Armus, Tanio Díaz-Santos, and Sabrina Stierwalt. *The Role of Star Formation and an AGN in Dust Heating of $z = 0.3\text{-}2.8$ Galaxies. I. Evolution with Redshift and Luminosity*. Research report no. 814:9. November 10, 2015. Accessed November 15, 2017.

<http://iopscience.iop.org/article/10.1088/0004-637X/814/1/9/meta;jsessionid=64983E953F2B18C5F729C919A383648F.c2.iopscience.cld>.

Lee, Nicholas, D. B. Sanders, Caitlin M. Casey, Sune Toft, N. Z. Scoville, Chao-Ling Hung, Emeric Le Floc'h, Olivier Ilbert, H. Jabran Zahid, and Hervé Aussel. *A Turnover in the Galaxy Main Sequence of Star Formation at $M^* \sim 10^{10} M_\odot$ for Redshifts $z < 1.3$* . Research report no. 801:80. March 5, 2015. Accessed November 15, 2017.

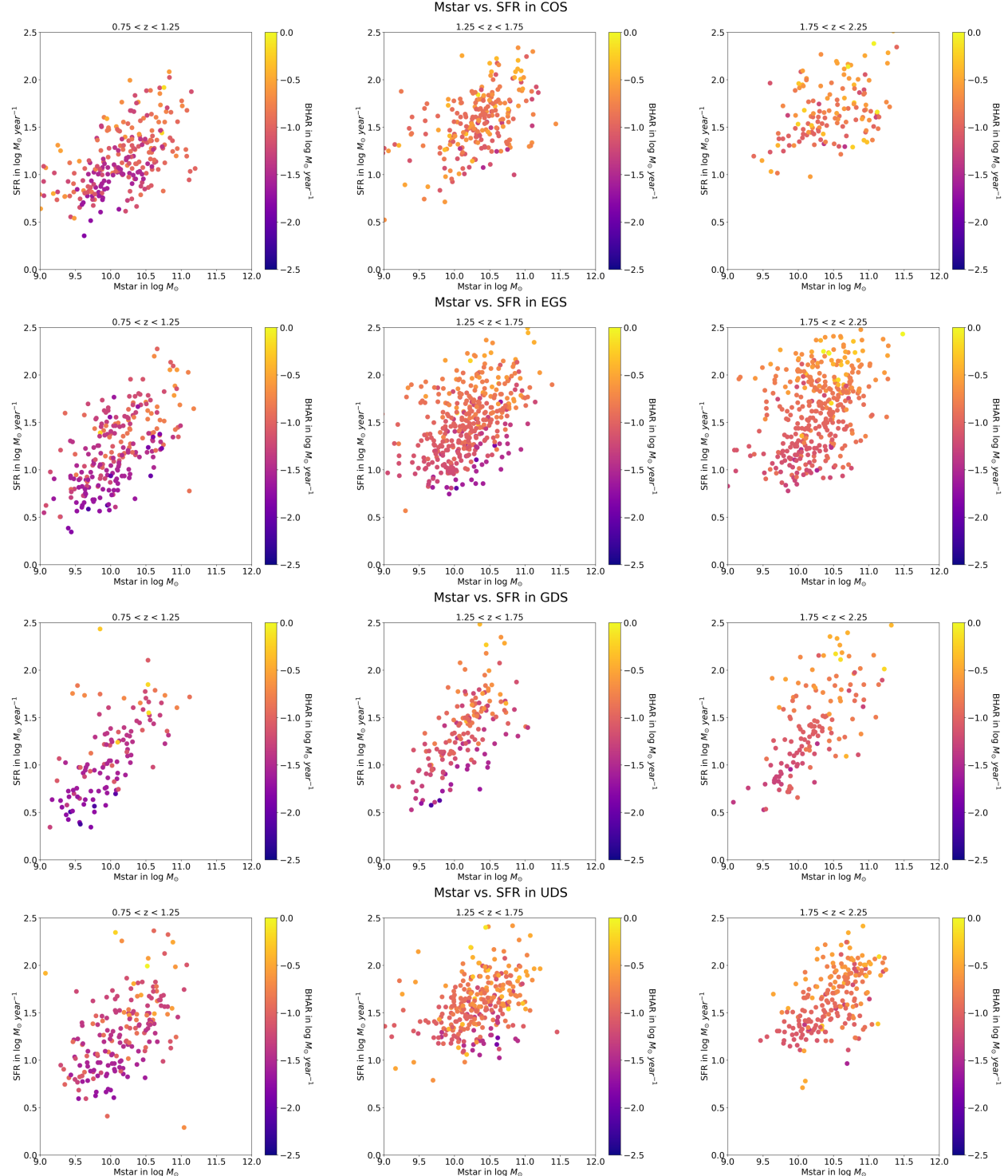
<http://iopscience.iop.org/article/10.1088/0004-637X/801/2/80/meta>.

Speagle, J. S., C. L. Steinhardt, P. L. Capak, and J. D. Silverman. *A Highly Consistent Framework for the Evolution of the Star-forming "Main Sequence" from $z \sim 0\text{-}6$* . Research report no. 214:15. September 18, 2014. Accessed November 15, 2017.

<http://iopscience.iop.org/article/10.1088/0067-0049/214/2/15/meta>.

Appendix

The following are Mstar vs. SFR plots for separate fields within CANDELS.



The following are Mstar vs. BHAR plots for separate fields within CANDELS.

